American Mineralogist, Volume 97, pages 1193–1198, 2012

A new cubic perovskite in $PbGeO_3$ at high pressures

Wansheng Xiao,[1,*] Dayong Tan,[1] Wei Zhou,[1] Ming Chen,[1,2] Xiaolin Xiong,[2] Maoshuang Song,[2] Jing Liu,[3] Ho-Kwang Mao,[4,5] and Jian Xu[6,7]

[1]Key Laboratory of Mineralogy and Metallogeny, Guangzhou Institute of Geochemistry, Chinese Academy of Sciences, Guangzhou 510640, China
[2]State Key Laboratory of Isotope Geochemistry, Guangzhou Institute of Geochemistry, Chinese Academy of Sciences, Guangzhou 510640, China
[3]Institute of High Energy Physics, Chinese Academy of Sciences, Beijing 100049, China
[4]Geophysical Laboratory, Carnegie Institution of Washington, Washington, D.C. 20015, U.S.A.
[5]High Pressure Collaborative Access Team, Carnegie Institution of Washington, Advanced Photon Source, Argonne National Laboratory, Argonne, Illinois 60439, U.S.A.
[6]Institute of Atomic and Molecular Physics, Sichuan University, Chengdu, 610065, China
[7]Institute of Fluid Physics, China Academy of Engineering Physics, Mianyang, 621900, China

Abstract

A new cubic perovskite polymorph of $PbGeO_3$ (Phase II) was synthesized by laser heating in the diamond-anvil cell (DAC) at the pressure of 36 GPa. Fitting the Birch-Murnaghan equation of state against its observed *P-V* data yields a bulk modulus K_0 of 196(6) GPa and the volume V_0 of 56.70(13) Å^3 when K_0' is assumed being 4. After the pressure is released, the $PbGeO_3$ Phase II changes gradually into an amorphous phase, which contains mainly fourfold-coordinated germanium. It indicates that the $PbGeO_3$ Phase II with a GeO_6 octahedron framework transforms to a GeO_4 tetrahedron network during the amorphization. The existence of $PbGeO_3$ cubic perovskite Phase II at high pressures indicates that the polarized character of the Pb^{2+} ion induced by its $6s^2$ lone pair electrons would be totally reduced in the environment of major silicate perovskites inside the lower mantle, and thus the Pb atom would substitute the Ca atom to enter the $CaSiO_3$ perovskite.

Keywords: Lead germanate, cubic perovskite, high pressure, amorphization

Introduction

The ABO_3 perovskite-structured oxides have been extensively investigated in geosciences, physics, chemistry, and material sciences. Many novel phase transitions in perovskite compounds have been thus discovered. For instance, the cubic $PbCrO_3$ perovskite (Phase I) transforms reversibly to another cubic perovskite (Phase II) with a 9.8% volume collapse at the pressure of ~1.6 GPa (Xiao et al. 2010); the multiferroic material of $PbVO_3$, which crystallizes in the polarized tetragonal perovskite (*P*4*mm*) structure at ambient conditions, changes reversibly to a cubic perovskite with >10% volume collapse at about 2 GPa (Belik et al. 2005); $BiCoO_3$ has the same polarized structure as $PbVO_3$ at ambient conditions but transforms to the orthorhombic perovskite (*Pnma*) with a 13% volume reduction at 3–4 GPa, which is induced by the high-spin to low-spin electronic transition in Co^{3+} cation and the complete suppression of the polarized character in the Bi^{3+} cation (Oka et al. 2010). Silicate perovskites are the primary mineral components in the Earth's lower mantle (Kesson et al. 1998; Wood 2000). Whether those novel phase transitions could appear in silicate perovskites or not is thus an intriguing topic in mineral crystal chemistry and mantle mineralogy. The Ge-O and Si-O bonds exhibit the similar covalent nature, and germanates and silicates appear to have similar structural characteristics and physical, chemical properties (Gibbs et al. 1998), therefore, germanates are considered as an analogs of silicates in high-pressure research.

$PbGeO_3$ crystallizes in the monoclinic pyroxenoid structure (*P*2/*n*, *Z* = 12) at ambient conditions. The lattice parameters are *a* = 11.469, *b* = 7.236, *c* = 12.555 Å, β = 113°18′, and *V* = 956.96 Å^3 (Nozik et al. 1979). It is the same structure as the natural mineral of alamosite ($PbSiO_3$) (Boucher and Peacor 1968). In the structure, the dominant feature is that a chain of the silicon (or germanium)-oxygen tetrahedra extends parallel to [10$\bar{1}$] and each chain has a lattice-translation repeat of 12 tetrahedral (Boucher and Peacor 1968). In addition, there is also a $PbGeO_3$ amorphous state ($PbGeO_3$ glass; labeled as Phase A1 below) when its melt is quenched at ambient pressure (Tomasi et al. 2005). At higher temperatures, the $PbGeO_3$ glass (Phase A1) transforms into an intermediate metastable crystalline modification at a temperature of about 430 °C and further to the stable monoclinic structure at above 570 °C (Tomasi et al. 2002). The structural details of this intermediate metastable modification remain unknown although it can be indexed as a hexagonal unit cell (Yamaguchi et al. 1985).

The investigation of pressure effects on structural behaviors of $PbGeO_3$ is scarce. When the intermediate hexagonal metastable modification of $PbGeO_3$ discussed above is compressed at room temperature, it undergoes an amorphization at 12–18 GPa with the coordination of Ge changing from 4 to 6 (Oelker et al. 2009). When the pressure is released, the high-pressure amorphous phase of $PbGeO_3$ transforms to a low-pressure amorphous phase with the sixfold coordination of Ge atoms reverting to fourfold, and the micro-structure of this decompressed amorphous material

* E-mail: wsxiao@gig.ac.cn

0003-004X/12/0007–1193$05.00/DOI: http://dx.doi.org/10.2138/am.2012.4021

is somewhat different from that of the melt-quenched $PbGeO_3$ glass (Oelker et al. 2009). This amorphous phase is therefore labeled as Phase A2 in this report. The $PbGeO_3$ was also investigated by high-pressure and high-temperature experiments with the large volume press (LVP) (Olekhnovich et al. 1994). The experimental pressure was in the range of 4–7 GPa and the temperature was from 1200 to 1800 K. The X-ray diffraction of the quenched samples indicates that there are three high-pressure polymorphs of $PbGeO_3$ existing meta-stably at ambient conditions. They are different from the low-pressure phases discussed above. The sequence of phases for $PbGeO_3$ with increasing pressures is as follows: monoclinic pyroxenoid structure ($P2/n$) → the tetragonal garnet phase ($I4_1/a$) → ilmenite phase ($R\bar{3}$) → cubic perovskite phase ($Pm3m$), which is similar to $CdGeO_3$ (Olekhnovich et al. 1994; Akaogi and Navrotsky 1987; Susaki 1989). The $PbGeO_3$ cubic perovskite (labeled as Phase I below) were synthesized at pressures of 6–7 GPa and high temperatures up to 1800 K (Olekhnovich et al. 1994).

Olekhnovich et al. (1994) noted that the volume (62.4 Å^3) of the cubic perovskite of $PbGeO_3$ (Phase I) at ambient conditions is larger by about 0.5% than that of its low-pressure ilmenite modification (62.1 Å^3). Normally, for most of the ABO_3 compounds appearing the pressure-induced phase transition from ilmenite to perovskite, the volume of the perovskite is smaller by about 5–10% than that of ilmenite (Susaki 1989). It seems that the lattice constant (a = 3.968 Å) of the cubic perovskite of $PbGeO_3$ (Phase I) synthesized by Olekhnovich et al. (1994) is abnormally large. From the point of view of crystal chemistry, the lattice constants of ABO_3-type perovskites mostly depend on their A- and B-cationic radii (Jiang et al. 2006; Ubic 2007); however, the lattice constant of ~3.968 Å in the $PbGeO_3$ cubic perovskite is much larger than that of the $SrGeO_3$ cubic perovskite (3.796 Å) (Shimizu et al. 1970), but is similar to that of $PbTiO_3$ (3.96 Å) (ICDD 40-0099), although the cationic radii of Sr^{2+} (1.44 Å) and Ti^{4+} (0.605 Å) are either little smaller or much larger than that of Pb^{2+} (1.49 Å) and Ge^{4+} (0.53 Å), respectively (Shannon 1976). Similarly at ambient conditions, the $PbCrO_3$ cubic perovskite ($PbCrO_3$ Phase I) also shows abnormally large lattice constant (4.013 Å), which transforms reversibly to another cubic perovskite ($PbCrO_3$ Phase II) at ~1.6 GPa with a 9.8% volume collapse (Xiao et al. 2010). We were thus expecting a much denser high-pressure cubic perovskite of $PbGeO_3$ to appear at higher pressures compared to the appearance of $PbCrO_3$ Phase II in the cubic perovskite $PbCrO_3$ system. Here we report this new cubic perovskite $PbGeO_3$ (labeled as below Phase II), which is observed at high pressures in our experiment. However, the new high-pressure $PbGeO_3$ cubic perovskite (Phase II) does not convert back to Phase I, but to an amorphous phase when the pressure is released to ~4 GPa and the amorphization is completed when the pressure is completely released.

Experimental methods

The raw material of monoclinic $PbGeO_3$ used as the high-pressure experimental sample was made by devitrification of $PbGeO_3$ glass (Phase A1, Scavini et al. 2001; Tomasi et al. 2002, 2005). The preparing process is as follows. Analytical grade PbO (99.99%) and GeO_2 (99.999%) were weighted with a mole ratio of 1.005:1 and mixed. The 0.5% excess of PbO is due to the slight evaporation of PbO at high temperature (Tomasi et al. 2002). The grounded mixture was melted within a platinum crucible in an electric furnace in air at 1100 °C. The melt was kept at this temperature for 1 h, then quenched by placing the crucible into a liquid nitrogen vessel to form the $PbGeO_3$ glass (Phase A1). A part of the prepared $PbGeO_3$ glass (Phase A1) was then annealed at 660 °C for 4 h and cooled down to room temperature by turning off the furnace. The X-ray diffraction pattern of the $PbGeO_3$ crystalline sample can be indexed as a monoclinic structure with the lattice parameters of a = 11.460(4), b = 7.237(3), c = 12.554(5) Å, β = 113.29(3)°, V = 956.40(43) Å^3. It is in good agreement with the single-crystal neutron diffraction results of the monoclinic $PbGeO_3$ (Nozik et al. 1979).

A symmetric Mao-Bell type diamond-anvil cell (DAC) was employed to generate the pressure. A pair of 400 μm culet-size diamond anvils was used in our experiments. A gasket was prepared by indenting a piece of T301 stainless steel foil to a thickness of about 40 μm; a 100 μm hole centered in the indentation served as the sample chamber. The monoclinic $PbGeO_3$ powder was pressed to a pellet with a thickness of about 15 μm, and a piece of sample about 60 μm in diameter was loaded into the sample chamber. Argon was used as a pressure-transmitting medium. It was cryogenically loaded into the sample chamber. It also served as the thermal-insulating medium during laser heating. A few fine ruby chips were loaded for in situ measurements of the sample pressure using the standard ruby fluorescence spectroscopy (Mao et al. 1986). The sample in the DAC was pressurized up to about 36 GPa and then heated by a YAG laser to temperatures of around 1500 to 2000 K. After heating, the pressure decreased to 35.4 GPa.

In situ high-pressure angle-dispersive X-ray diffraction (ADXD) experiments were performed at the 4W2 beamline of Beijing synchrotron radiation facility (BSRF). An image plate detector (MAR-345) was used to collect the diffraction patterns. The wavelength of the monochromatic X-ray beam is 0.6199 Å calibrated by scanning through the Mo metal K-absorption edge. The X-ray beam was focused to a beam size of 20 (vertical) × 30 (horizontal) μm^2 full-width at half maximum (FWHM) by a pair of Kirkpatrick-Baez mirrors. The distance between the sample and the detector was calibrated to be 350.04 mm by using CeO_2 as a standard. All of the ADXD patterns were collected in the decompressed process from 35.4 GPa to 0.1 MPa at room temperature without further annealing. The collected diffraction patterns were analyzed by integrating images as a function of 2θ using the program Fit2D (Hammersley et al. 1996) to obtain a conventional, one dimensional diffraction profile.

The sample recovered from high pressure, the melt-quenched $PbGeO_3$ glass (Phase A1), and the monoclinic $PbGeO_3$ crystal was analyzed by Raman scattering at ambient conditions. Raman spectra were recorded by a Renishaw 2000 micro-Raman spectrometer in the backscattering geometry. An argon ion laser operating at the line of 514.5 nm was used as the exciting source. A thermoelectrically cooled CCD detector was equipped to collect the scattered light dispersed by an 1800 lines/mm grating. Raman spectra were collected over the 100–1100 cm^{-1} range.

Results

Figure 1 exhibits several X-ray diffraction (XRD) patterns of $PbGeO_3$, which has been produced at ~36 GPa with the laser-heating. These patterns were collected at different pressures between 4.7 and 35.4 GPa. In each of these patterns, besides the diffraction peaks belonging to the pressure medium of argon, there are only six reflection peaks, which can be perfectly indexed into a simple cubic structure. No characteristic peaks from other impurities can be detected from these XRD data, which indicates that the synthesis product has high purity. When the pressure is released to 4.7 GPa, the XRD patterns show no obvious change but each of these diffraction peaks shifts to the lower diffraction angle. The d-spacings and lattice constants of the synthesized cubic phase of $PbGeO_3$ at several representative pressures are shown in Table 1. The cell volumes indicate that there is only one chemical formula of $PbGeO_3$ in each unit cell, and thus the single cubic phase of $PbGeO_3$ is concluded to be the cubic perovskite structure ($Pm3m$). The structural refinements of 35.4 GPa and 4.7 GPa XRD patterns with the GSAS package (Toby 2001), as shown in Figure 1, also supports the conclusion.

When the pressure is further decreasing from 4.7 GPa to atmospheric pressure, the $PbGeO_3$ cubic perovskite transforms gradually to an amorphous state. This behavior is similar to that

of $CaSiO_3$ perovskite (Mao et al. 1989; Wang et al. 1996). Figure 2 shows the low-pressure XRD patterns from 3.8 GPa down to atmospheric pressure, which described the amorphous process of the $PbGeO_3$ cubic perovskite, in which the dotted lines indicate the pressure effects on the broad and weak diffraction peaks of the amorphous sample. When the pressure is released to 3.8 GPa, a weak broad peak appears at ~2.93 Å, which indicates the occurrence of the amorphization. The intensity of the 2.93 Å peak increases gradually at the expense of the diffraction intensity of the $PbGeO_3$ cubic perovskite in the decompression process, and it becomes the most intense peak. At the same time, the original diffraction peaks from the $PbGeO_3$ cubic perovskite become very weak at 2.4 GPa and completely disappear at 1.6 GPa. During the amorphization process, besides the appearance of the most intense and broad diffraction peak at ~3 Å, some other weak peaks also gradually appear with decompression. At atmospheric pressure, these peaks can be observed at 5.15, 4.00, 3.13, 2.73, and 2.32 Å, as shown in Figure 2. The weak peaks may represent a small amount of nano-sized crystals or pre-nucleated centers in the amorphous matrix, as observed in the pressure-amorphized materials of $PbGeO_3$ (Oelker et al. 2009).

This amorphous sample unloaded from the $PbGeO_3$ cubic perovskite high-pressure experiment (labeled as Phase A2 below) was used for Raman measurement to reveal its micro-structural characteristics. For comparison, the monoclinic $PbGeO_3$ crystalline and the Phase A1 samples were also analyzed by the Raman technique. The results are shown in Figure 3. We can see that the Raman spectrum of the Phase A2 sample is similar to that of Phase A1 (the melt-formed glass) but substantially different

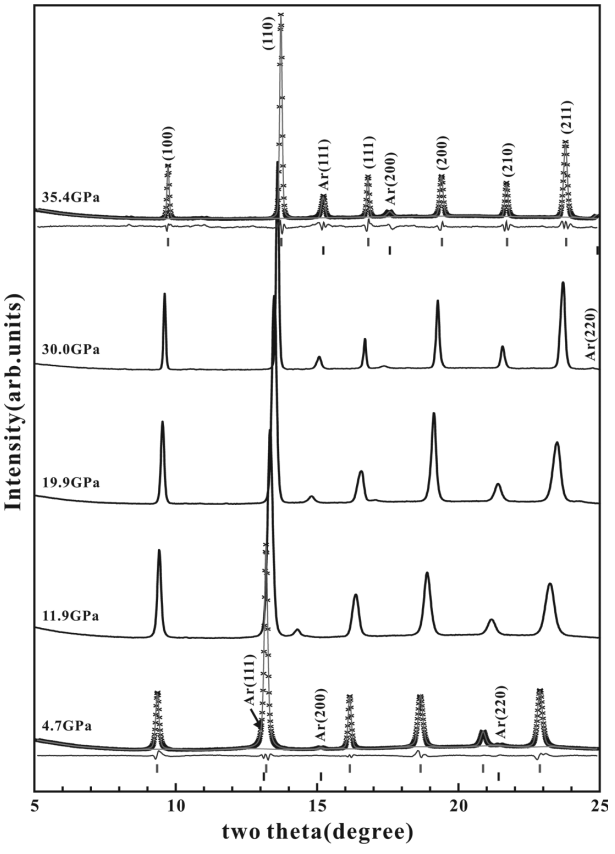

FIGURE 1. X-ray powder diffraction patterns for $PbGeO_3$ cubic perovskite (Phase II) at several pressures. The 4.7 and 35.4 GPa fitting patterns from the Rietveld analysis are also superimposed in the figure.

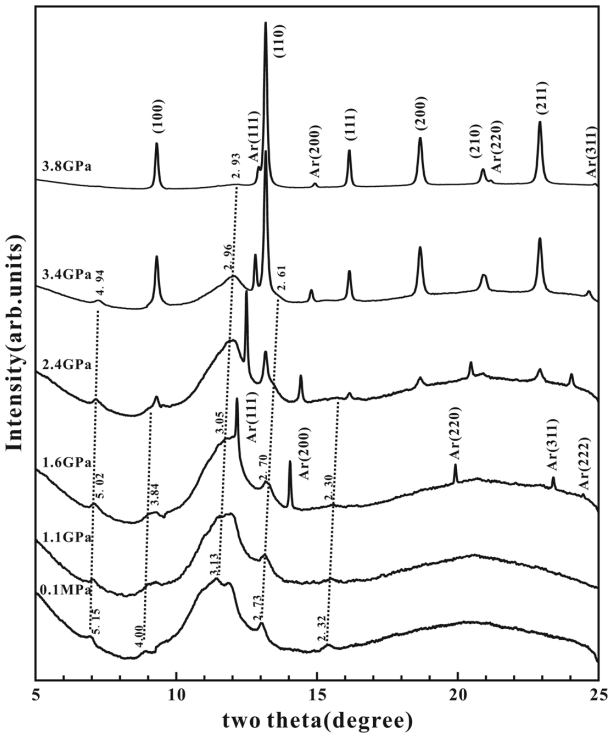

FIGURE 2. X-ray powder diffraction patterns at pressures between 0–3.8 GPa showing the pressure-released amorphous process of the $PbGeO_3$ cubic perovskite (Phase II). The dotted lines indicate the pressure effects on the broad and weak diffraction peaks of the amorphous sample. The weak peaks may represent a small amount of nano-sized crystal or pre-nucleated center in the amorphous matrix.

TABLE 1. *d*-spacings and lattice parameters of $PbGeO_3$ cubic perovskite at different pressures

	35.4 GPa			4.7 GPa			2.4 GPa		
	d_{obs} (Å)	d_{calc} (Å)	d_{obs}-d_{calc} (Å)	d_{obs} (Å)	d_{calc} (Å)	d_{obs}-d_{calc} (Å)	d_{obs} (Å)	d_{calc} (Å)	d_{obs}-d_{calc} (Å)
(100)	3.6692(3)	3.6696	–0.0004	3.8163(3)	3.8169	–0.0006	3.8248(14)	3.8231	0.0017
(110)	2.5938(1)	2.5948	–0.0010	2.6985(1)	2.6990	–0.0005	2.7016(3)	2.7034	–0.0018
(111)	2.1191(1)	2.1187	0.0004	2.2041(1)	2.2037	0.0004	2.2058(5)	2.2073	–0.0015
(200)	1.8356(4)	1.8348	0.0008	1.9092(1)	1.9085	0.0007	1.9109(4)	1.9116	–0.0007
(210)	1.6415(4)	1.6411	0.0004	1.7077(3)	1.7070	0.0007	1.7122(11)	1.7098	0.0025
(211)	1.4988(1)	1.4981	0.0007	1.5584(2)	1.5583	0.0001	1.5599(6)	1.5608	–0.0009
a (Å)	3.6696(5)			3.8169(4)			3.8231(11)		
V (Å^3)	49.42(2)			55.61(2)			55.88(5)		

Note: The numbers in the parentheses are the estimated standard deviations.

from that of the monoclinic $PbGeO_3$. The two disorder phases show several broad Raman bands; however, the crystalline $PbGeO_3$ contains more than 20 sharp bands indicating its low symmetry. In the two amorphous samples, although their spectra show little differences, the strong broad bands of 793 and 727 cm^{-1} indicate that the disorder network contains predominantly fourfold-coordinated germanium (Oelker et al. 2009). The obvious discrepancies between Phase A1 and Phase A2 appear mainly in the low-wavenumber area. A band of 250 cm^{-1} emerges in Phase A2 while it is absent in Phase A1. The most intense band in the amorphous material (Phase A2) is at 124 cm^{-1}, which is assigned as symmetric stretching vibrations of Pb-O either in square pyramids or in trigonal pyramids with Pb atoms in the apex (Sigaev et al. 2001); while in Phase A1 we observe two partially overlapping bands at 117 and 132 cm^{-1}. The Raman evidences indicate that the $PbGeO_3$ cubic perovskite undergoes amorphization by transforming the corner-linked GeO_6 octahedra framework to the disordered GeO_4 tetrahedra network, and the micro-structure of Phase A2 is a little different from Phase A1.

Table 2 lists all of the unit-cell volume data of the $PbGeO_3$ cubic perovskite obtained at different pressures in this study, and those pressure-volume data are plotted in Figure 4. In this diagram, the atmosphere-pressure volume of the $PbGeO_3$ cubic perovskite (Phase I) determined by Olekhnovich et al. (1994) is also plotted. Obviously, the $PbGeO_3$ cubic perovskite (Phase I) identified by Olekhnovich et al. (1994), which was produced at about 6–7 GPa and high temperatures by LVP, is much different from the one (Phase II) we observed in our DAC experiment in this study due to the large volume difference.

Fitting the Birch-Murnaghan equation of state to all the *P-V* data for $PbGeO_3$ Phase II yields initial bulk modulus $K_0 = 198(4)$ GPa and unit-cell volume $V_0 = 56.66(9)$ Å^3 if the initial pressure derivative of the bulk modulus K_0' is fixed to 4. However, from the *P-V* data of $PbGeO_3$ Phase II in Figure 4, we can find that the 4 low-pressure volumes at 2.4 to 3.8 GPa deviate somewhat from the experimental *P-V* trend showing a little smaller volume. Wang et al. (1996) observed a significant decrease in volume of $CaSiO_3$ cubic perovskite as the pressure is lowered from 1 to 0.59 GPa and attributed it to the effect of the amorphization. This volume effect was also observed as the $(Mg,Fe)SiO_3$ perovskites were heated at the ambient pressure associating with its amorphization (Wang et al. 1994). The $PbGeO_3$ Phase II begins its amorphization at about 3.8 GPa, thus the anomalous volumes are probably associated to this process. For this reason we have performed a new fit without using the four lowest pressure data. This yields an initial bulk modulus (K_0) of 196(6) GPa and a zero-pressure volume (V_0) of 56.70(13) Å^3 with a fixed bulk modulus pressure derivative (K_0') as 4. The fitted zero-pressure volume of $PbGeO_3$ Phase II is smaller by about 9.1% than the observed volume ($V_0 = 62.4$ Å^3) of Phase I, this situation is somewhat similar to the volume difference between Phase I and Phase II in $PbCrO_3$ (Xiao et al. 2010).

TABLE 2. Experimental pressure-volume data of $PbGeO_3$ cubic perovskite

Pressure (GPa)	Volume (Å^3)
2.4(0.1)	55.88(5)
2.9(0.1)	55.74(2)
3.4(0.2)	55.70(3)
3.8(0.2)	55.70(2)
4.7(0.2)	55.61(2)
5.7(0.3)	55.33(2)
6.5(0.3)	55.08(3)
7.9(0.4)	54.69(4)
9.5(0.5)	54.23(4)
11.9(0.6)	53.52(3)
14.0(0.7)	52.99(1)
16.2(0.8)	52.55(2)
18.0(0.9)	52.19(1)
19.9(1.0)	51.95(2)
21.6(1.1)	51.59(3)
23.7(1.2)	51.34(2)
25.8(1.3)	51.07(2)
28.2(1.4)	50.76(1)
30.0(1.5)	50.56(2)
32.0(1.6)	50.06(4)
33.5(1.7)	49.57(2)
35.4(1.8)	49.42(2)

Notes: The estimated standard deviations of the fitted unit-cell volume are given in parentheses. The uncertainties of pressure given in parentheses are estimated to be 5% of relative error based on the ruby technique in this study.

The pressure-volume relationship in Figure 4 displays a slightly anomalous volume change at pressures between 30 and 32 GPa. It is attributed to the uncertainty of the pressure determination in this pressure region. Because the ruby chip we used was relatively large ~10 μm, the bridging effect makes a large pressure uncertainty (~5%) in this pressure region although normally the error of the pressure determination in the ruby technique is within 1%.

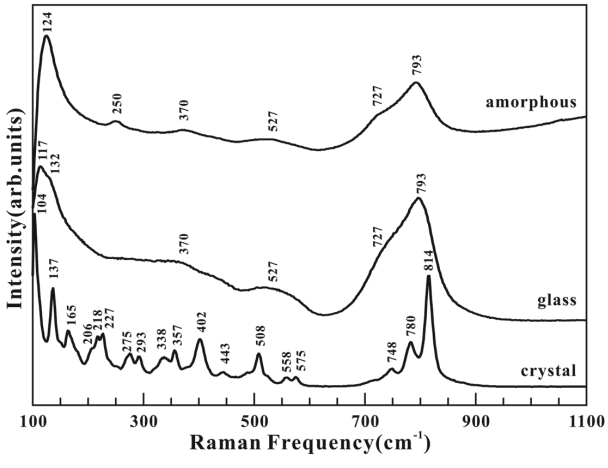

FIGURE 3. Raman spectra of the pressure-quenched amorphous, melt-quenched glassy, and monoclinic crystalline states of $PbGeO_3$. All spectra were collected at ambient conditions.

DISCUSSION

It is rare that a compound has two different stable polymorphs with the same structure but different volumes at different pressure and temperature conditions. To our knowledge, this kind of phenomenon appears only in few materials. The isostructural phase transitions are usually considered to be originating from an electronic structural change in the matters; such transitions appear in cubic Ce (γ-α) (Hall et al. 1964), SmS (B1) (Maple and Wohlleben 1971), and hexagonal MnO (B8) (Yoo et al. 2005) at room temperature and 0.7, 0.65, and ~110 GPa with the volume reductions of 15.0, 13.6, and 6.6%, respectively. The transitions of γ-α in Ce and B1-B1 in SmS occur when the localized *f*-electron becomes delocalized (Lipp et al. 2008; Barla et al. 2004); the B8-B8 transition in MnO is considered as

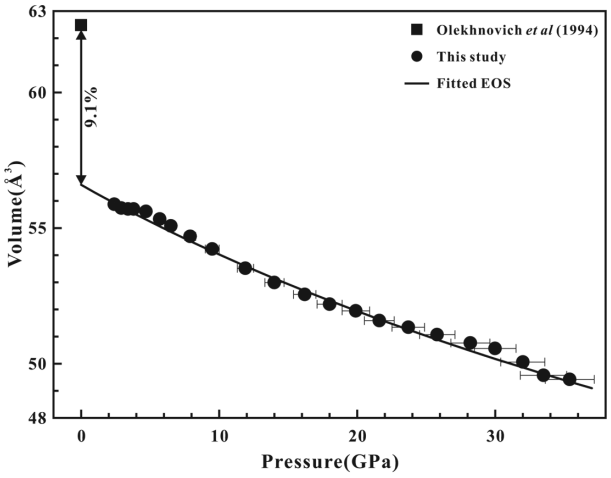

FIGURE 4. Pressure-volume relationship of the $PbGeO_3$ cubic perovskites. The solid cycles represent the observed data of the $PbGeO_3$ Phase II, and the solid square indicates the volume of the $PbGeO_3$ Phase I at ambient conditions. The solid curve is the Birch-Muraghan equation of state fit with K_0 = 196(6) GPa, V_0 = 56.70(13) Å^3, and an assumed K_0' = 4. Notice that at pressures below 4 GPa, the unit-cell volumes deviate from the experimental *P-V* tendency showing a little reduced volume, which is associated with the amorphization. The estimated standard deviations (e.s.d.) of the unit-cell volume (see Table 2) are smaller than the size of the symbols. The error bars of pressure show the estimated 5% uncertainties of pressure determination in the ruby technique in this study.

a high-spin to low-spin transition of the Mn ions (Kuneš et al. 2008). Thus, it is of scientific interest that there are possibly two cubic perovskite high-pressure polymorphs with a large volume difference also in the $PbGeO_3$ compound. However, unlike for the reversible phase transition between the cubic perovskite $PbCrO_3$ (I) and $PbCrO_3$ (II) at ~1.6 GPa, in the case of the cubic perovskite $PbGeO_3$ (Phase II), the back transformation to Phase I (Olekhnovich et al., 1994) does not occur, instead an amorphous phase appears when the pressure is released to atmospheric pressure. Neither experimental description nor diffraction details have been reported in the sole source of $PbGeO_3$ (I) (Olekhnovich et al. 1994). Therefore, more convincing and detailed experimental evidences are needed for $PbGeO_3$ (I).

For most of the germanate compounds including the GeO_6 octahedron, the average Ge-O bond length is in the range of 1.89–1.91 Å (Shimizu et al. 1970; Sasaki et al. 1983; Susaki 1989; Umesaki et al. 1995; Yusa et al. 2006). At 2.4 GPa, the lowest pressure of $PbGeO_3$ Phase II appearing in this study, the Ge-O bond distance in $PbGeO_3$ Phase II is 1.910 Å. According to the extrapolated atmosphere pressure volume (56.70 Å^3), the Ge-O bond length in the $PbGeO_3$ Phase II at ambient conditions should be 1.921 Å, a little larger than the average Ge-O bond length in a typical GeO_6 octahedron. The little larger Ge-O bond distance in $PbGeO_3$ Phase II is related to the larger Pb^{2+} ionic radius owing to the correlated Ge-O and Pb-O bonds. However, the $PbGeO_3$ Phase I has an exceptional large Ge-O bond distance of 1.984 Å (Olekhnovich et al. 1994). Similarly, $PbCrO_3$ Phase I also exhibits the abnormal Cr-O bond distance, which lead to its anomalous compressibility and the unusual isostructural transition (Xiao et al. 2010). It would be very interesting to verify whether the $PbGeO_3$ Phase I has a similar behavior and transforms to Phase II at high pressure or not.

Based on the lattice constant statistics on the 132 cubic and pseudo-cubic perovskites, an empirical relations were deduced to predict the lattice constants of possible cubic perovskite structure through the ion radius (Jiang et al. 2006; Moreira and Dias 2007; Ubic 2007). Ubic (2007) suggested an improved formula:

$$a_{calc} = 0.06741 + 0.490523(r_A + r_X) + 1.29212(r_B + r_X)$$

where r_A and r_B are the radii of the A and B cations, respectively, and r_X is the radius of the anion. Under ambient conditions, the extrapolated zero-pressure lattice constant of the $PbGeO_3$ Phase II of 3.842 Å agrees well with the empirical relationship (3.832 Å, with a deviation of 0.26%), whereas the lattice constant (3.968 Å) of the $PbGeO_3$ Phase I is far beyond that of the formula. The deviation (3.43%) from the formula is also much larger than the average deviation (0.60%) for these kinds of cubic perovskites.

Table 3 lists the bulk moduli of some perovskite-structured compounds. The zero-pressure bulk modulus of $PbGeO_3$ Phase II is comparable to that of $SrGeO_3$ and $CaGeO_3$ germanate perovskites, the Pb-containing cubic perovskites of $PbCrO_3$ Phase II and $PbTiO_3$, but is smaller than that of $MgGeO_3$ and $ZnGeO_3$ perovskites. It is also smaller than that of cubic $CaSiO_3$ and orthorhombic $MgSiO_3$ perovskites. It suggests that the $PbGeO_3$ Phase II exhibits the normal compressibility and thus it is a "normal" cubic perovskite.

Different from the alkaline earth cations of Mg^{2+}, Ca^{2+}, and Sr^{2+}, which exhibit prominent ionic character, the Pb^{2+} cation shows strong polarization due to its $6s^2$ lone-pair electrons, and usually forms covalent bonds with oxygen atom at ambient conditions (Trinquire and Hoffmann 1984; Häussermann et al. 2001). The Pb-based oxide perovskites, such as $PbTiO_3$ and $PbVO_3$ (Sani et al. 2002; Belik et al. 2005), also crystallize in the distorted tetragonal perovskite structure (*P4mm*) at ambient conditions for the polarized character of the Pb^{2+} cation. The normal compressibility of the $PbGeO_3$ cubic perovskite Phase II indicates that the polarized character of Pb^{2+} cation is completely suppressed when Pb^{2+} combines with Ge^{4+} to form the oxide perovskite at high pressures. Accordingly, we speculate that Pb^{2+} could combine with Si^{4+} to form a cubic perovskite other than dissolving into the oxide mixtures in the lower mantle. In addition, based on the lattice strain model (Blundy and Wood

TABLE 3. Comparison of bulk modulus of $PbGeO_3$ cubic perovskite with that of relative compounds with perovskite structure

	Structure	K_0	K_0'	Ref
$PbGeO_3$	Cubic	196(6)	4	This study
$SrGeO_3$	Cubic	189	4.8	Akaogi et al. (2005)
$CaGeO_3$	Orthorhombic	194(2)	6.1	Ross and Angel (1999)
$MgGeO_3$	Orthorhombic	216(3)	4	Runge et al. (2006)
$ZnGeO_3$	Orthorhombic	250(3)	4	Yusa et al. (2006)
$PbCrO_3$	Cubic	59(5)*	4	Xiao et al. (2010)
	Cubic	187(4)†	4	
$PbTiO_3$	Cubic	195(3)	4	Sani et al. (2002)
$CaSiO_3$	Cubic	232(8)	4.8	Wang et al. (1996)
$MgSiO_3$	Orthorhombic	253(9)	3.9	Fiquet et al. (2000)

Note: The estimated standard deviations of the bulk moduli are given in parentheses.
* Low-pressure Phase I.
† High-pressure Phase II.

1994), the Pb atom would substitute the Ca atom to enter the $CaSiO_3$ perovskite, one of the mineralogical components in the Earth's mantle (Kesson et al. 1998; Wood 2000).

ACKNOWLEDGMENTS

We gratefully acknowledge the help from High-Pressure Beam Line, BSRF, China. The work has been supported by the National Natural Science Foundation of China (11179030, 90714011, 41090373), the Knowledge Innovation Project of the Chinese Academy of Sciences (KJCX2-SW-N20), the Research Foundation of China Academy of Engineering Physics under Grant No. 2008A0101001, and the Research Foundation of National Key Laboratory of Shock Wave and Detonation Physics under Grants No. 9140C6703010703 and 9140C6703010803. This is contribution No. IS-1460 from GIGCAS.

REFERENCES CITED

Akaogi, M. and Navrotsky, A. (1987) Calorimetric study of high-pressure phase transitions among the $CdGeO_3$ polymorphs (pyroxenoid, garnet, ilmenite, and perovskite structures). Physics and Chemistry of Minerals, 14, 435–440.

Akaogi, M., Kojitani, H., Yusa, H., Yamamoto, R., Kido, M., and Koyama, K. (2005) High-pressure transitions and thermochemistry of $MGeO_3$ (M = Mg, Zn and Sr) and Sr-silicates: Systematics in enthalpies of formation of $A^{2+}B^{4+}O_3$ perovskites. Physics and Chemistry of Minerals, 32, 603–613.

Barla, A., Sanchez, J.P., Haga, Y., Lapertot, G., Doyle, B.P., Leupold, O., Rüffer, R., Abd-Elmeguid, M.M., Lengsdorf, R., and Flouquet, J. (2004) Pressure-induced magnetic order in golden SmS. Physical Review Letters, 92, 066401.

Belik, A.A., Azuma, M., Saito, T., Shimakawa, Y., and Takano, M. (2005) Crystallographic features and tetragonal phase stability of $PbVO_3$, a new member of $PbTiO_3$ family. Chemistry of Materials, 17, 269–273.

Blundy, J. and Wood. B. (1994) Prediction of crystal-melt partition coefficients from elastic moduli. Nature, 372, 452–454.

Boucher, M.L. and Peacor, D.R. (1968) The crystal structure of alamosite, $PbSiO_3$. Zeitschrift für Kristallographie, Bd. 126, S. 98–111.

Fiquet, G., Dewaele, A., Andrault, D., Kunz, M., and LeBihan, T. (2000) Thermoelastic properties and crystal structure of $MgSiO_3$ perovskite at lower mantle pressure and temperature conditions. Geophysical Research Letters, 27, 21–24.

Gibbs, G.V., Boisen, M.B., Hill, F.C., Tamada, O., and Downs, R.T. (1998) SiO and GeO bonded interactions as inferred from the bond critical point properties of electron density distributions. Physics and Chemistry of Minerals, 25, 574–584.

Hall, H.T., Merrill, L., and Barnett, J.D. (1964) High pressure polymorphism in cesium. Science, 146, 1297–1299.

Hammersley, A.P., Svensson, S.O., Hanfland, M., Fitch, A.N., and Hausermann, D. (1996) Two-dimensional detector software: From real detector to idealised image or two-theta scan. High Pressure Research, 14, 235–248.

Häussermann, U., Berastegui, P., Carlson, S., Haines, J., and Léger, J. (2001) TlF and PbO under high pressure: Unexpected persistence of the stereochemically active electron pair. Angewandte Chemie International Edition, 40, 4624–4629.

Jiang, L.Q., Guo, J.K., Liu, H.B., Zhu, M., Zhou, X., Wu, P., and Li, C.H. (2006) Prediction of lattice constant in cubic perovskites. Journal of Physics and Chemistry of Solids, 67, 1531–1536.

Kesson, S.E., Fitz Gerald, J.D., and Shelley, J.M.G. (1998) Mineralogy and dynamics of a pyrolite lower mantle. Nature, 393, 252–255.

Kuneš, J., Lukoyanov, A.V., Anisimo, V.I., Scalettar, R.T., and Pickett, W.E. (2008) Collapse of magnetic moment drives the Mott transition in MnO. Nature Materials, 7, 198–202.

Lipp, M.J., Jackson, D., Cynn, H., Aracne, C., Evans, W.J., and McMahan, A.K. (2008) Thermal signatures of the Kondo volume collapse in cerium. Physical Review Letters, 101, 165703.

Mao, H., Xu, J., and Bell, P.M. (1986) Calibration of the ruby pressure gauge to 800 kbar under quasi-hydrostatic conditions. Journal of Geophysical Research, 91, 4673–4676.

Mao, H., Chen, L., Hemley, R., Jephcoat, A., Wu, Y., and Bassett, W. (1989) Stability and equation of state of $CaSiO_3$-perovskite to 134 GPa. Journal of Geophysical Research, 94, 17889–17894.

Maple, M.B. and Wohlleben, D. (1971) Nonmagnetic 4f shell in the high-pressure phase of SmS. Physical Review Letters, 27, 511–515.

Moreira, R.L. and Dias, A. (2007) Comment on "Prediction of lattice constant in cubic perovskites." Journal of Physics and Chemistry of Solids, 68, 1617–1622.

Nozik, Yu.Z., Maksimov, B.A., Fykin, L.E., Dudarev, V.Ya., Garashina, L.S., and Gabrielyan, V.T. (1979) Neutron diffraction study of lead germanate $PbGeO_3$. Journal of Structural Chemistry, 19, 628–630.

Oelker, E.N., Bhat, M.H., Soignard, E., and Yargeret, J.L. (2009) Pressure-induced transformations in crystalline and vitreous $PbGeO_3$. Solid State Communications, 149, 1940–1943.

Oka, K., Azuma, M., Chen, W.T., Yusa, H., Belik, A.A., Takayama-Muromachi, E., Mizumaki, M., Ishimatsu, N., Hiraoka, N., Tsujimoto, M., Tucker, M.G., Attfield, J.P., and Shimakawa, Y. (2010) Pressure-induced spin-state transition in $BiCoO_3$. Journal of the American Chemical Society, 132, 9438–9443.

Olekhnovich, N.M., Salak, A.N., Zhabko, T.E., Savchuk, V.K., and Shilin, A.D. (1994) $PbGeO_3$ structure phase-transitions under high-pressures and temperatures and ferroelectric perovskites of the $PbZrO_3$-$PbGeO_3$ system. Doklady Akademii Nauk Belarusi, 38, 40–44 (in Russian).

Ross, N.L. and Angel, R.J. (1999) Compression of $CaTiO_3$ and $CaGeO_3$ perovskites. American Mineralogist, 84, 277–281.

Runge, C.E., Kubo, A., Kiefer, B., Meng, Y., Prakapenka, V.B., Shen, G., Cava, R.J., and Duffy, T.S. (2006) Equation of state of $MgGeO_3$ perovskite to 65 GPa: Comparison with the post-perovskite phase. Physics and Chemistry of Minerals, 33, 699–709.

Sani, A., Hanfland, M., and Levy, D. (2002) The equation of state of $PbTiO_3$ up to 37 GPa: A synchrotron X-ray powder diffraction study. Journal of Physics-Condensed Matter, 14, 10601–10604.

Sasaki, S., Prewitt, C.T., and Liebermann, R.C. (1983) The crystal structure of $CaGeO_3$ perovskite and the crystal chemistry of $GdFeO_3$-type perovskites. American Mineralogist, 68, 1189–1198.

Scavini, M., Tomasi, C., Speghini, A., and Bettinelli, M. (2001) Stable and metastable phases within the GeO_2-rich part of the binary PbO-GeO_2 system. Journal of Materials Synthesis and Processing, 9, 93–102.

Shannon, R.D. (1976) Revised effective ionic radii and systematic studies of interatomic distances in halides and chalcogenides. Acta Crystallographica, A32, 751–767.

Shimizu, Y., Syono, Y., and Akimoto, S. (1970) High-pressure transformations in $SrGeO_3$, $SrSiO_3$, $BaGeO_3$, and $BaSiO_3$. High Temperatures-High Pressures, 2, 113–120.

Sigaev, V.N., Gregora, I., Pernice, P., Champagnon, B., Smelyanskaya, E.N., Aronne, A., and Sarkisov, P.D. (2001) Structure of lead germinate glasses by Raman spectroscopy. Journal of Non-Crystalline Solids, 279, 136–144.

Susaki, J.I. (1989) $CdGeO_3$-phase transformations at high pressure and temperature and structural refinement of the perovskite polymorph. Physics and Chemistry of Minerals, 16, 634–641.

Toby, B.H. (2001) EXPGUI, a graphical user interface for GSAS. Journal of Applied Crystallography, 34, 210–213.

Tomasi, C., Scavini, M., Speghini, A., Bettinelli, M., and Riccardi, M.P. (2002) Devitrification kinetics of $PbGeO_3$: Isothermal and non-isothermal study. Journal of Thermal Analysis and Calorimetry, 70, 151–164.

Tomasi, C., Scavini, M., Cavicchioli, A., Speghini, A., and Bettinelli, M. (2005) Isothermal and non-isothermal kinetic study of the $PbGeO_3$ solid-solid phase transition. Thermochimca Acta, 432, 2–9.

Trinquire, G. and Hoffmann, R. (1984) Lead monoxide. Electronic structure and bonding. The Journal of Physical Chemistry, 88, 6696–6711.

Ubic, R. (2007) Revised method for the prediction of lattice constants in cubic and pseudocubic perovskites. Journal of the American Ceramic Society, 90, 3326–3330.

Umesaki, N., Brunier, T.M., Wright, A.C., Hannon, A.C., and Sinclair, R.N. (1995) Neutron scattering from PbO-GeO_2 glasses. Physica B, 213–214, 490–492.

Wang, Y., Weidner, D.J., Liebermann, R.C., and Zhao, Y. (1994) P-V-T equation of state of $(Mg,Fe)SiO_3$ perovskite: Constraints on composition of the lower mantle. Physics of the Earth and Planetary Interiors, 83, 13–40.

Wang, Y., Weidner, D., and Guyot, F. (1996) Thermal equation of state of $CaSiO_3$ perovskite. Journal of Geophysical Research, 101, 661–672.

Wood, B.J. (2000) Phase transformations and partitioning relations in peridotite under lower mantle conditions. Earth and Planetary Science Letters, 174, 341–354.

Xiao, W., Tan, D., Xiong, X., Liu, J., and Xu, J. (2010) Large volume collapse observed in the phase transition in cubic $PbCrO_3$ perovskite. Proceedings of the National Academy of Sciences, 107, 14026–14029.

Yamaguchi, O., Sugiura, K., Muto, M., and Shimizu, K. (1985) Compound formation in the System $PbGeO_3$-$Pb_3Ge_3O_{11}$. Zeitschrift für Anorganische und Allgemeine Chemie, 525, 230–236.

Yoo, C.S., Maddox, B., Klepeis, J.H.P., Iota, V., Evans, W., McMahan, A., Hu, M.Y., Chow, P., Somayazulu, M., Häusermann, D., Scalettar, R.T., and Pickett, W.E. (2005) First-order isostructural Mott transition in highly compressed MnO. Physical Review Letters, 94, 115502.

Yusa, H., Akaogi, M., Sata, N., Kojitani, H., Yamamoto, R., and Ohishi, Y. (2006) High-pressure transformations of ilmenite to perovskite, and lithium niobate to perovskite in zinc germinate. Physics and Chemistry of Minerals, 33, 217–226.

MANUSCRIPT RECEIVED OCTOBER 9, 2011
MANUSCRIPT ACCEPTED MARCH 26, 2012
MANUSCRIPT HANDLED BY SERGIO SPEZIALE